Silicon (2020) 12:193–198
https://doi.org/10.1007/s12633-019-00113-9

ORIGINAL PAPER

Ultra-Wideband Photonic Hybrid Plasmonic Horn Nanoantenna with SOI Configuration

Abbas Nourmohammadi[1] · Mahmoud Nikoufard[2]

Received: 15 August 2018 / Accepted: 15 February 2019 / Published online: 25 April 2019

Abstract
The current study proposes a hybrid plasmonic horn-like nanoantenna with a silicon-on-insulator (SOI) configuration. This nanoantenna can be utilized for broadband nanophotonic applications and can operate in a wide optical frequency range of 160–400 THz. It includes optical communication wavelengths of 850, 1310 and 1550 nm. This nanoantenna can directionally radiate and receive signals with about 74% bandwidth within the operational wavelength spectrum. The proposed nanoantenna is simulated using the finite element method and produced nanoantenna gains of 4.7, 7.3 and 4.8 dB and a reflection coefficient (S_{11}) of −15.7, −12.8 and −15.6 dB at optical wavelengths of 1550, 1310 and 850 nm, respectively.

Keywords Horn nanoantenna · Hybrid plasmonic waveguide · Silicon-on-insulator · Photonic integrated circuit · Wideband optical nanoantenna

1 Introduction

To compact photonic integrated circuits toward the nanoscale, several types of nanoscale waveguides have been investigated on a silicon-on-insulator (SOI) platform. Two such waveguides are photonic crystals [1–6] and surface plasmon waveguides [7–10]. The dielectric properties of noble metal can cause surface-plasmon resonance in the visible and infrared (IR) spectrums. The surface plasmon waveguides support highly localized optical fields at the interface of the metal-dielectric layer, so that surface plasmon polaritons propagate at the planar interface.

Optical antennas efficiently convert free-propagating optical radiation into localized energy and vice versa [11]. Therefore, the potential applications of optical antennas are closely related to their ability to strongly localize optical fields. With the help of surface plasmon resonance theory and antenna theory, researchers are advancing new methods of designing new optical antennas [12–14]. Various shapes for the optical antennas have been inspired by the designs of microwave antennas, such as the dipole or bow-tie [15], Yagi-Uda [16], spiral [17], horn [18–20], J-pole and V-shaped [21] and tapered-slot [22]. To design an optical antenna for optical wireless communications, the parameters of gain, directivity, reflection coefficient and antenna impedance should be taken into account [10, 23–25].

In this work, we focused on a configuration that is able to operate in a range of optical frequencies by using a new SOI-based horn-shaped nanoantenna. This nanoantenna is broadband at a wider range of frequencies (160–400 THz) in comparison with the previous antennas [10, 25]. This nanoantenna is capable of radiating all three optical communication wavelengths of 1550 nm (193.5 THz), 1310 nm (229 THz) and 850 nm (352.9 THz) with slightly higher gains at all wavelengths and smaller dimensions. All the features make this nanoantenna a good candidate for energy-harvesting applications or integration with devices such as dual laser combiner modules in communication systems.

2 SOI-Based HP-Waveguide Horn Nanoantenna

The proposed nanoantenna consists of a SOI-based hybrid plasmonic waveguide that is connected to a horn-like configuration. A schematic of the horn nanoantenna is shown in Fig. 1a. As seen, the layer structure of the waveguide

✉ Mahmoud Nikoufard
mnik@kashanu.ac.ir

[1] Nanoscience and Nanotechnology Center, University of Kashan, Kashan 8731753153, Iran

[2] Department of Electronics, University of Kashan, Kashan 8731753153, Iran

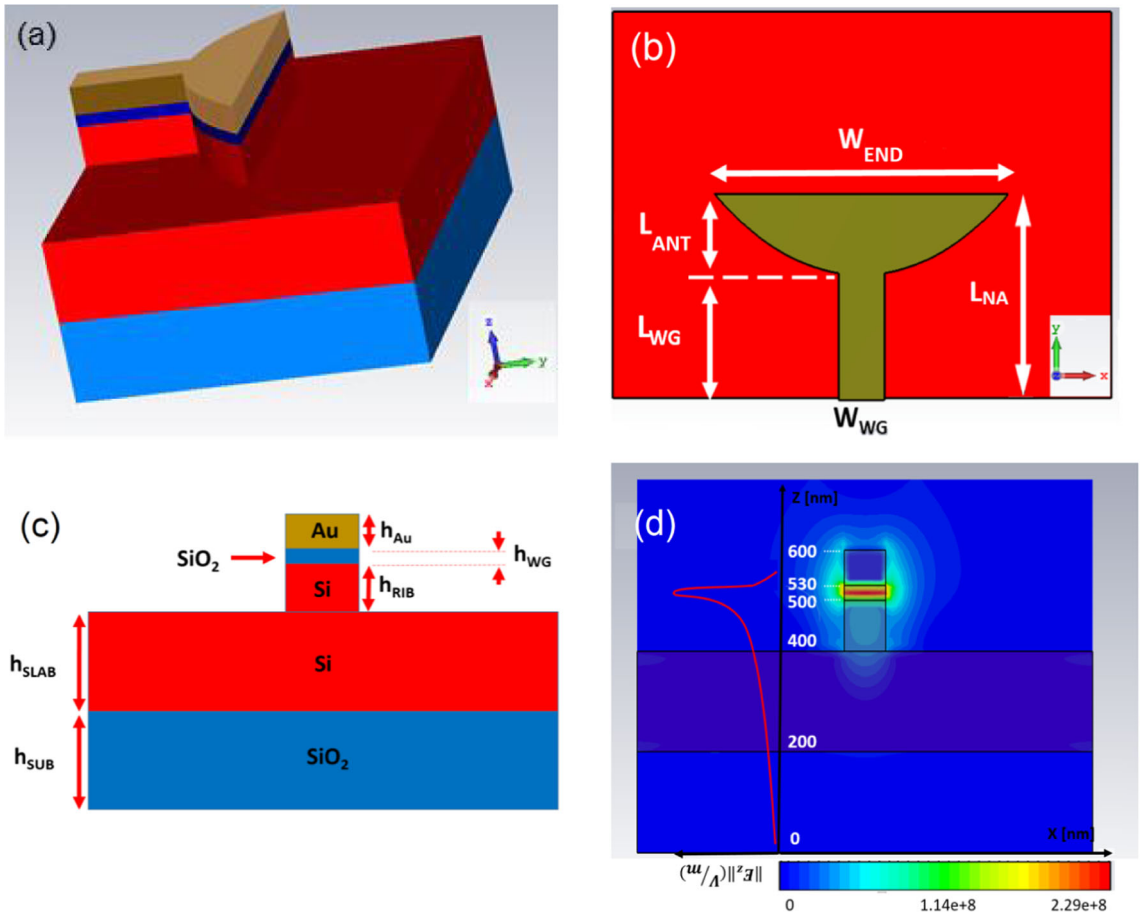

Fig. 1 **a** 3D view of horn nanoantenna; **b** top view of horn nanoantenna; **c** lateral 2D cross-section of input HP-waveguide; **d** norm of electric field distribution in lateral cross-section of input HP waveguide with norm of E-field along z-axis at the middle of waveguide ridge

and horn-nanoantenna are the same, so this configuration is suitable for monolithic integration with the SOI-based passive photonic integrated circuits. In addition, the layer stack used in the proposed nanoantenna is compatible with the complementary metal-oxide-semiconductor (CMOS) technology which makes the fabrication of the proposed device feasible. The horn-nanoantenna is an ellipsoidal configuration which is connected to the hybrid plasmonic (HP) waveguide (Fig. 1b).

Figure 1c shows that the SiO_2-cladding layer is sandwiched between a metal cap layer and a partly-etched Si layer. The thicknesses of these layers were set at $h_{WG} = 30$ nm, $h_{Au} = 70$ nm, and $h_{RIB} = 100$ nm, respectively. The layered structure is taken from Yousefi [10] in which the authors have proposed a rectangular patch optical nanoantenna to radiate the optical field from a hybrid plasmonic waveguide. When comparing the simulation results with Saad-Bin-Alam [25], which is a SOI-based broadband bowtie nanoantenna, the maximum footprint of the nanoantenna is set to 800 × 1100 nm, but, we have substituted a silver for a gold cap layer because the surface plasmon resonance of the material is more adapted to the working frequency of ref. [26].

The horn-nanoantenna was simulated using finite integration technique (FIT) with computer simulation technology (CST) in

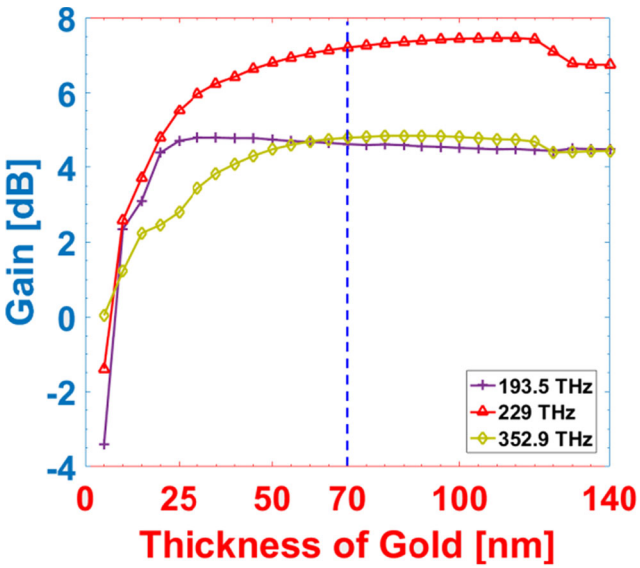

Fig. 2 Gain versus capped gold layer thickness at operating frequencies of 193.5 THz (1550 nm), 229 THz (1310 nm) and 352.9 THz (850 nm)

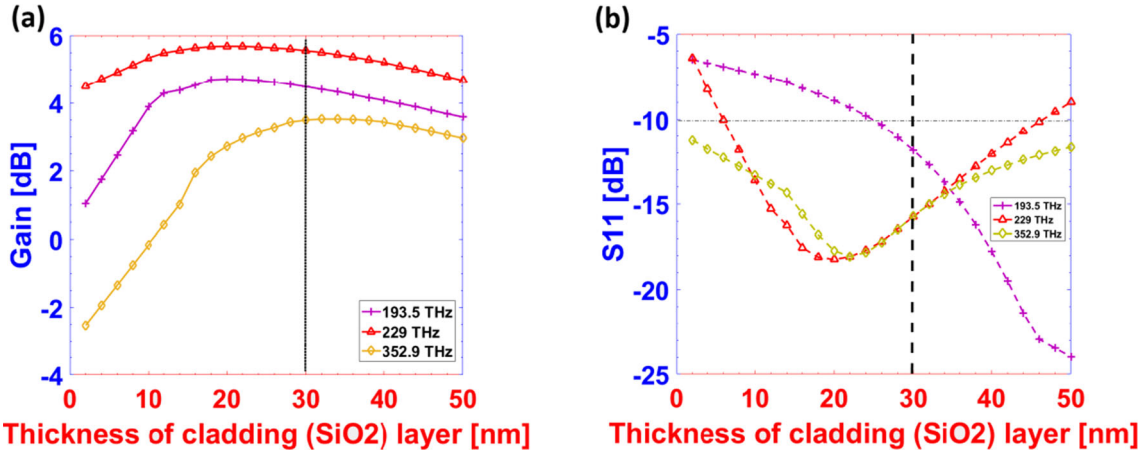

Fig. 3 **a** Gain versus cladding layer thickness at $h_{Au} = 70$ nm and $h_{RIB} = 100$ nm along the positive y-axis; **b** S_{11} versus SiO_2 cladding layer thickness at frequencies of 193.5, 229 and 352.9 THz

Microwave Studio software. The input fundamental transverse magnetic (TM) field is launched into the input port. Figure 1d shows the calculated modal electric field (z-component of electric field, $|E_z|$) in the input port of the horn nanoantenna. It can be observed that the optical field is confined in the thin SiO_2 layer between a metallic cap layer and a highly refractive index Si layer. To support the fundamental TM mode and provide a perfect impedance match between the antenna and the waveguide, the width of the SiO_2-cladding layer (W_{WG}) was chosen as 100 nm. The relative permittivity of SiO_2, Si and Au were extracted from ref. (http://refractiveindex.info), Palik [27] and Johnson [28], respectively.

The optimum thickness of the gold and cladding layers as well as the input waveguide length were numerically calculated. Figure 2 shows that the nanoantenna gain was negative for a gold thickness (h_{Au}) of less than 10 nm at working frequencies of 193.5, 229 and 352.9 THz due to the longer penetration depth of light into the gold layer at these frequencies [29]. For the thicker metal layer, the gain also increased, but for the thickness values of >70 nm, the gain was a very gradual increase at operating frequencies of 352.99 and 193.5 THz. Therefore, the $h_{Au} = 70$ nm value was chosen as the metal cap layer thickness.

Figure 3a shows very low and negative gains for the very thin SiO_2 layer ($h_{WG} < 10$ nm) at operating frequencies of 229 and 352.9 THz. Because light waves penetrates to the Si core and SiO_2 substrate layers, it cannot propagate in the desired direction. By increasing the thickness of the SiO_2 cladding layer, the gain for all three frequencies improved. A gradual decrease in gain can be observed for the SiO_2 layer thickness of >30 nm. To choose an optimum value, a desirable value for S_{11} must also be achieved. Figure 3b shows that the S_{11} is less than −10 dB for the SiO_2 layer thickness of >25 nm. Thus, a thickness for the SiO_2 cladding layer of 30 nm was chosen to provide sufficient gain and $S_{11} < -10$ dB.

Table 1 Optimization of variables L_{WG}, L_{NA} and W_{END}

Variables	Min value	Max value	Optimized value
L_{WG}	50 [nm]	400 [nm]	275 [nm]
L_{NA}	300 [nm]	800 [nm]	450 [nm]
W_{END}	200 [nm]	1100 [nm]	625 [nm]

3 Analytical Modeling of Nanoantenna

To determine the optimum dimensions of a nanoantenna, the following variables were optimized using the trust region

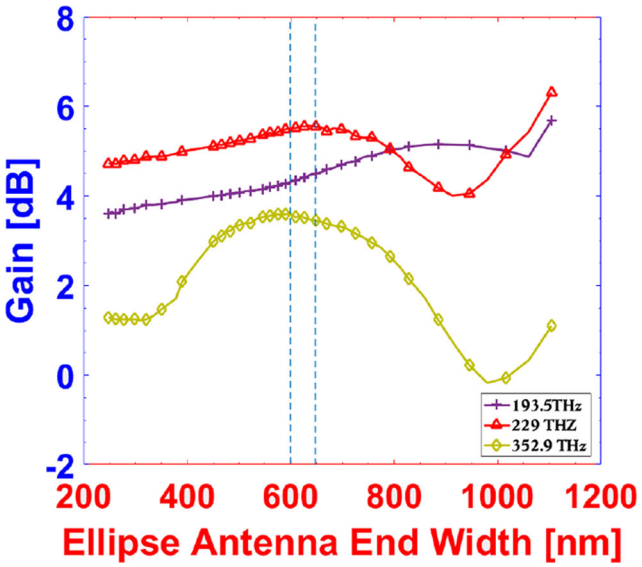

Fig. 4 Gain versus nanoantenna aperture width (W_{END}) in positive y-axis direction at frequencies of 193.5, 229 and 352.9 THz. The dashed lines show the maximum widths at working frequencies of 352.9 and 229 THz, respectively

framework method in CST Microwave Studio: overall length of nanoantenna (L_{NA}), length of waveguide (L_{WG}) and width of nanoantenna aperture (W_{END}). Table 1 provides details about the optimization results.

The minimum and maximum L_{NA}, L_{WG}, and W_{END} values were based on several criteria. The maximum L_{NA} and W_{EnD} values were 800 and 1100 nm, respectively, to make it substantially greater than $\lambda_c/2 = 535.5$ nm ($\lambda_c = 1071$ nm). The maximum substrate dimensions were 1100 × 800 nm to compare the simulation results with ref. [25]. The minimum waveguide length and total antenna length were 50 and 300 nm, respectively, to produce the low S_{11} at the optical wavelength windows [30]. By setting the optimization goals to reach a maximum gain and $S_{11} < -10$ dB at operating frequencies of 193.5, 229 and 352.9 THz, the optimum values of $L_{WG} =$ 275 nm, $L_{NA} = 450$ nm and $W_{END} = 625$ nm were obtained.

Figure 4 shows the gain of the horn nanoantenna as a function of the width of the nanoantenna aperture (W_{END}). The simulation results show that the maximum gain was obtained for aperture widths of $W_{END} = 600$ and 650 nm at working frequencies of 352.9 and 229 THz, respectively. $W_{END} = 625$ nm was chosen as the optimum value for this simulation and the other parameters were kept constant ($L_{WG} = 275$ nm, $L_{NA} = 450$ nm).

The 3D far-field radiation pattern at optical wavelengths of 1550 nm (193.5 THz), 1310 nm (229THz) and 850 nm (352.9THz) and a reflection coefficient (S_{11}) through the broadband frequency range of 150–400 THz are shown in Fig. 5. Figure 5a to c show that the radiation patterns of the proposed nanoantenna are directed toward the positive *y*-axis with gains of 4.7, 7.3 and 4.8 dB at optical wavelengths of 1550, 1310 and 850 nm, respectively. The simulation results show a higher gain and lower dimensions in comparison with the SOI-based broadband hybrid bowtie nanoantenna [25]. The S_{11} graph in Fig. 5d reveals that the proposed nanoantenna can radiate optical waves into free space at a frequency range of 160–400 THz with a bandwidth of around 74%. This bandwidth can cover the desired optical communication wavelengths.

Figure 6 shows the electrical field distributions of the horn nanoantenna at optical wavelengths of 1550, 1310 and 850 nm. The input HP-waveguide is illuminated in the fundamental TM mode (Fig. 1d) which is concentrated in the SiO_2 cladding layer. The incident wave propagates through the

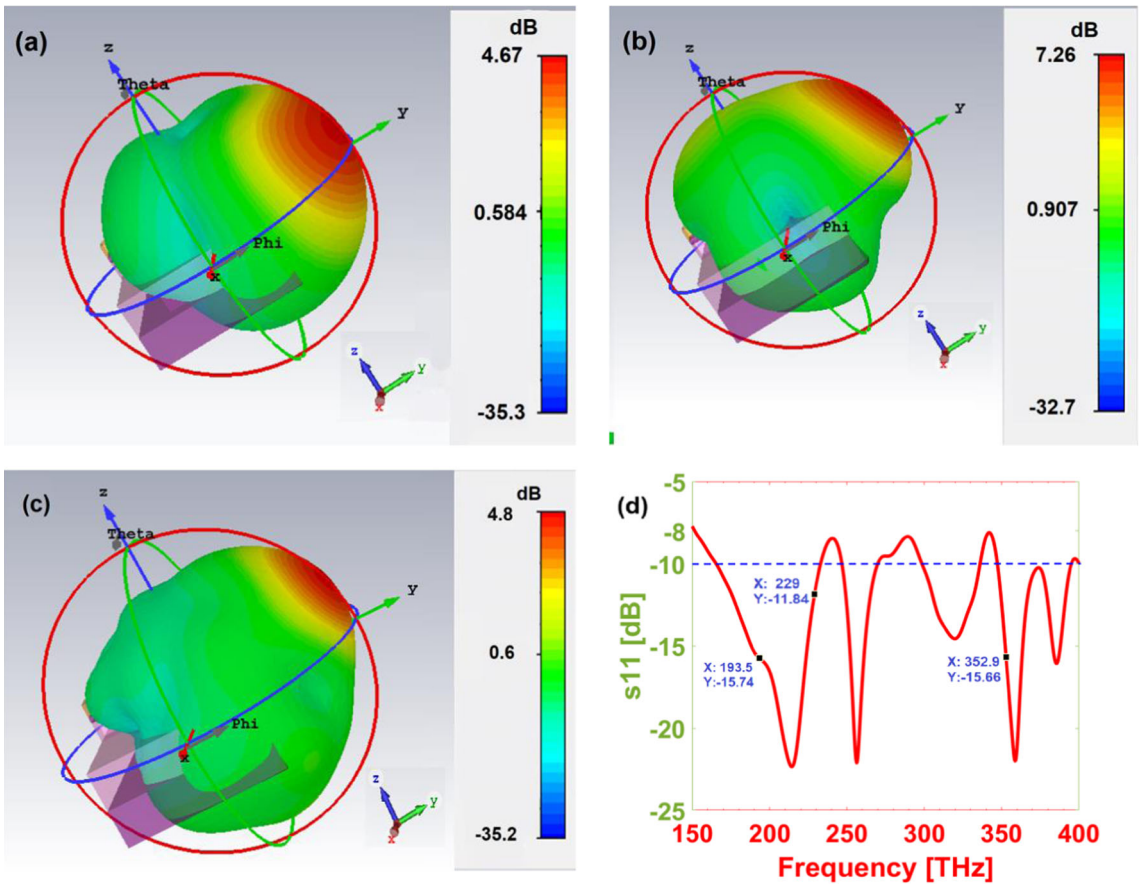

Fig. 5 3D radiation patterns of proposed broadband horn nanoantenna for optical wavelengths of: **a** 1550 nm (193.5 THz); **b** 1310 nm (229 THz); **c** 850 nm (352.9 THz); **d** reflection coefficient (S_{11}) versus incident optical wave frequency. The dimensions of the horn-nanoantenna was based on optimized values listed in Table 1. The other parameters are: $h_{WG} =$ 30 nm, $h_{Au} = 70$ nm, $W_{WG} = 100$ nm

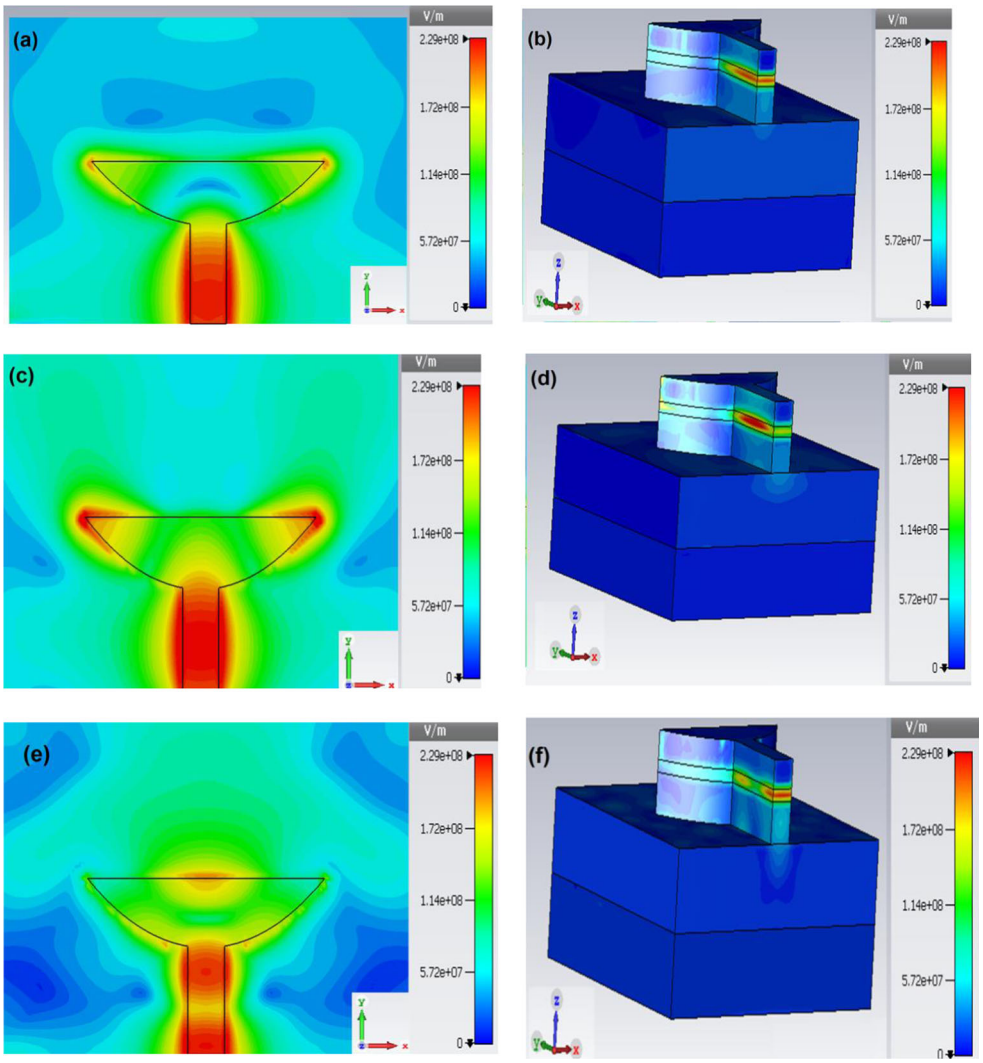

Fig. 6 2D cross-section of E-field distributions in the middle of the SiO_2 cladding layer for **a** $\lambda = 1550$ nm; **c** $\lambda = 1310$ nm; **e** $\lambda = 850$ nm. 3D view of E-field distributions of the nanoantenna for: **b** $\lambda = 1550$ nm; **d** $\lambda = 1310$ nm; **f** $\lambda = 850$ nm

straight HP-waveguide and radiates to free space through the horn nanoantenna. Figure 6b, d and f show 3D views of the horn nanoantenna with the electrical field distributions at different layers. A better view of the *E*-field distribution shows the 2D cross-section of the hybrid plasmonic nanoantenna in the middle of the SiO_2-cladding layer for all the three wavelengths (Fig. 6a, c and e).

4 Conclusions

The proposed horn broadband nanoantenna can operate in an infra/optic range from 160 to 400 THz. With satisfactory gains for all the optical communication wavelength windows of 1550, 1310 and 850 nm, this nanoantenna is a good candidate for infrared/optical frequencies. The proposed device can be used in different nanophotonic applications, especially for inter- and intra-chip optical communications to establish a wireless-optical link between the optical circuits. The proposed nanoantenna can also be used for optical energy harvesting (nanorectenna or nantenna) and optical-sensing because of its wide frequency coverage. It also is possible to reduce the size as well as cost by monolithic integration with the passive photonic integrated devices. The footprint of the proposed nanoantenna is 450 × 625 nm.

References

1. Elsayed HA, Aly AH (2017) Terahertz frequency superconductor-nanocomposite photonic band gap. Int J Mod Phys B 32(05): 1850056
2. Aly AH, Sayed H (2017) Enhancement of the solar cell based on nanophotonic crystals. J Nanophotonics 11(4):046020
3. Aly AH, Sabra W, Elsayed HA (2017) Cutoff frequency in metamaterials photonic crystals within Terahertz frequencies. Int J Mod Phys B 31(15):1750123
4. Aly AH (2008) Metallic and superconducting photonic crystal. J Supercond Nov Magn 21(7):421–425

5. Aly AH, Mehaney A, El-Naggar SA (2017) Evolution of phononic band gaps in one-dimensional phononic crystals that incorporate high-Tc superconductor and magnetostrictive materials. J Supercond Nov Magn 30(10):2711–2716
6. Aly AH, Sabra W (2016) Superconductor-semiconductor metamaterial photonic crystals. J Supercond Nov Magn 29(8): 1981–1986
7. Vivien L, Osmond J, Fédéli JM, Marris-Morini D, Crozat P, Damlencourt JF, Cassan E, Lecunff Y, Laval S (2009) 42 GHz pin Germanium photodetector integrated in a silicon-on-insulator waveguide. Opt Express 17(8):6252–6257
8. Aalto T, Solehmainen K, Harjanne M, Kapulainen M, Pi H (2006) Low-loss converters between optical silicon waveguides of different sizes and types. IEEE Photon Technol Lett 18(5):709–711
9. Dai D, He S (2009) A silicon-based hybrid plasmonic waveguide with a metal cap for a nano-scale light confinement. Opt Express 17(19):16646–16653
10. Yousefi L, Foster AC (2012) Waveguide-fed optical plasmonic patch nano-Antenna. Frontiers in optics, optical society of America, p FTh3A. 4
11. Balanis CA (1992) Antenna theory: a review. Proc IEEE 80(1):7–23
12. Alù A, Engheta N (2008) Hertzian plasmonic nanodimer as an efficient optical nanoantenna. Phys Rev B 78:195111
13. Sederberg S, Elezzabi AY (2011) Sierpiński fractal plasmonic antenna: a fractal abstraction of the plasmonic bowtie antenna. Opt Express 19:10456–10461
14. Dregely D, Lindfors K, Lippitz M, Engheta N, Totzeck M, Giessen H (2014) Imaging and steering an optical wireless nanoantenna link. Nat Commun 5:4354
15. Pan Z, Guo J (2013) Enhanced optical absorption and electric field resonance in diabolo metal bar optical antennas. Opt Express 21: 32491–32500
16. Dregely D, Taubert R, Dorfmüller J, Vogelgesang R, Kern K, Giessen H (2011) 3D optical Yagi–Uda nanoantenna array. Nat Commun 2:267
17. Singh R, Rockstuhl C, Menzel C, Meyrath TP, He M, Giessen H, Lederer F, Zhang W (2009) Spiral-type terahertz antennas and the manifestation of the Mushiake principle. Opt Express 17:9971–9980
18. Grosjean T, Mivelle M, Burr GW, Baida FI (2013) Optical horn antennas for efficiently transferring photons from a quantum emitter to a single-mode optical fiber. Opt Express 21:1762–1772
19. Ramaccia D, Bilotti F, Toscano A, Massaro A (2011) Efficient and wideband horn nanoantenna. Opt Lett 36:1743–1745
20. Ramaccia D, Bilotti F, Toscano A, Massaro A, Cingolani R (2011) Electrical and radiation properties of a horn nano-antenna at near infrared frequencies. Antennas and Propagation (APSURSI), 2011 IEEE International Symposium on. IEEE, pp 2407–2410
21. James TD, Davis TJ, Roberts A (2014) Optical investigation of the J-pole and Vee antenna families. Opt Express 22:1336–1341
22. Guo H, Meyrath TP, Zentgraf T, Liu N, Fu L, Schweizer H, Giessen H (2008) Optical resonances of bowtie slot antennas and their geometry and material dependence. Opt Express 16:7756–7766
23. Malheiros-Silveira GN, Wiederhecker GS, Hernández-Figueroa HE (2013) Dielectric resonator antenna for applications in nanophotonics. Opt Express 21:1234–1239
24. Nikoufard M, Nourmohammadi A, Esmaeili S (2018) Hybrid plasmonic nanoantenna with the capability of monolithic integration with laser and photodetector on InP-substrate. IEEE Trans Antennas Propag 66:3–8
25. Saad-Bin-Alam M, Khalil MI, Rahman A, Chowdhury AM (2015) Hybrid plasmonic waveguide fed broadband nanoantenna for nanophotonic applications. IEEE Photon Technol Lett 27:1092–1095
26. Solati E, Dorranian D (2015) Comparison between silver and gold nanoparticles prepared by pulsed laser ablation in distilled water. J Clust Sci 26:727–742
27. Palik ED (1998) Handbook of optical constants of solids. Academic Press
28. Johnson PB, Christy RW (1972) Optical constants of the noble metals. Phys Rev B 6:4370–4379
29. Kreibig U, Vollmer M (2013) Optical properties of metal clusters, vol 25. Springer Science & Business Media
30. Novotny L (2007) Effective wavelength scaling for optical antennas. Phys Rev Lett 98:266802